

**SESSION VII**

**Diesel Engine Technologies for Emission Reduction II**

**Session Chair: Mike Nazemi**

**SCAQMD**

# Si/Si<sub>0.8</sub>Ge<sub>0.2</sub> AND B<sub>4</sub>C/B<sub>5</sub>C QUANTUM WELLS THERMOELECTRIC FOR DIESEL ENGINES

S. Ghamaty and N. Elsner  
Hi-Z Technology, San Diego, California, U.S.A.

## ABSTRACT

The electronic and thermal properties of bulk materials are altered when they are incorporated into quantum wells. Two-dimensional quantum wells have been synthesized by alternating layers of B<sub>4</sub>C and B<sub>5</sub>C in one system and alternating layers of Si and Si<sub>0.8</sub>Ge<sub>0.2</sub> in another system. Such nanostructures are being investigated as candidate thermoelectric materials for high figures of merit (Z). The predicted enhancement is attributed to the confined motion of charge carriers and phonons in the two dimensions and separating them from the ion scattering centers.

Molecular beam epitaxy (MBE) and sputtering techniques have been used to prepare these multilayer films. Films have been deposited on single-crystal silicon substrates. The  $\alpha$  and  $\rho$  properties of these films have been determined over a broad range of temperatures from 4.2K to 1200K and were previously reported. The  $\alpha^2/\rho$  values for these P type B-C and N type SiGe films were more than a factor of 10 to 30 times higher than bulk P type B-C and N type SiGe.

Recently, thermal conductivities have also been measured with a modified 3- $\omega$  method. The room temperature thermal conductivity of Si and Si<sub>0.8</sub>Ge<sub>0.2</sub> were also encouraging smaller, and about one third (1/3) of the bulk values and in line with theoretical predictions. The performance of the MBE films have been systematically compared with bulk materials. Preliminary thermoelectric measurements of the multilayer structures, lead us to believe that significant gains in the thermoelectric figure of merit (Z) may be possible with this approach.

The first quantum well thermoelectric couple with N-type Si/Si<sub>0.8</sub>Ge<sub>0.2</sub> and P-type B<sub>4</sub>C/B<sub>5</sub>C was fabricated from these films. The test results generated continue to indicate that much higher thermoelectric efficiencies can be achieved in the quantum wells compared to the bulk materials. Also, the potential cost of fabricating quantum well modules will be discussed and are expected to be much lower than present bulk thermoelectric module on a cost/watt basis.

## BACKGROUND

Thermoelectric materials are utilized for power generation in remote locations, on spacecraft used for interplanetary exploration, and in places where waste heat can be recovered. Broader usage is limited by the efficiency of present systems and the power-specific cost (\$/W) of power generation. Materials with a  $ZT \geq 6$  can lead to a factor of 2 to 3 improvement in thermodynamic efficiency. Recall that the thermodynamic efficiency,  $\eta$ , of a thermoelectric power generator is

$$\eta = \frac{T_h - T_c}{T_h} \left[ \frac{M - 1}{M + T_c/T_h} \right] \quad (1)$$

where M is defined as

$$M = \sqrt{1 + \frac{1}{2} Z (T_c + T_h)} \quad (2)$$

and  $T_h$  is the absolute temperature at the hot junction and  $T_c$  is the absolute temperature at the cold junction. To achieve a high efficiency with a power generator, the overall figure of merit for the device, Z, must be high. The figures of merit of the thermoelectric materials used to construct the device must also be high. For a specific material, Z is defined as:

$$Z = \frac{\sigma \alpha^2}{\kappa_{ph} + \kappa_{el}} \quad (3)$$

where  $\sigma$  is the electrical conductivity,  $\alpha$  is the Seebeck coefficient,  $\kappa_{ph}$  is the phonon contribution to the thermal conductivity, and  $\kappa_{el}$  is the electronic contribution to the thermal conductivity. Note that  $\kappa_{ph}$  is also known as  $\kappa_L$ , the lattice thermal conductivity. Much of the effort to improve Z over the past 20-30 years has focused on attempts to reduce  $\kappa$ , without adversely affecting the electrical conductivity. Some success has been achieved with solid-solution alloying. Further reductions in

$\kappa_L$  have been achieved by reducing the grain size of silicon-germanium alloys, however, this approach is still in its infancy and the potential benefit is believed to be relatively small.

Multilayer films of  $B_4C/B_8C$  and  $Si/Si_{0.8}Ge_{0.2}$  are being investigated as a means of achieving a high Z. Models based upon quantum mechanics predict that such structures should have an unusually high Z [1-5]. The quantum-well (QW) layer is sandwiched between two barrier layers. Typically, the QW material has a very narrow band gap and the barrier material has a relatively large band gap. Molecular beam epitaxy (MBE) and sputtering have been employed to fabricate the samples.

For power applications, the concern is that the above materials will inter-diffuse at some elevated temperature and lose their two-dimension structure and associated quantum well properties. For power generation applications, B-C and SiGe alloys appeared to be the best initial selection for the following reasons:

- B-C have very low diffusion coefficients in one another.
- Si and Ge have very low diffusion coefficients in one another. The dopants boron and phosphorous however can diffuse much quicker and high temperature aging studies will be necessary to determine how long these films will remain stable at the anticipated operating temperatures.
- B-C as well as SiGe alloys do not have to be deposited in an exact stoichiometry to be useful thermoelectric materials.
- Since stoichiometry is not critical, the deposition process can be conducted with less critical controls.

## EXPERIMENTAL

### $\alpha$ and $\rho$ Measurements

Room temperature resistivities were measured on samples using the following method: the current was introduced at the ends of a long, rectangular cut sample and the voltage probes were near the center of the test specimen. The resistance was obtained from the voltage drop, and the resistivity was calculated by knowing the cross-sectional area of the bar and the distance between the two voltage probes (ASTM F-43). The Alleis instrument, which uses pressure contacts, was used as the voltage probes in this case.

The high temperature  $\alpha$  and  $\rho$  of the films were measured in a system at HI-Z and the results have been published previously [4, 5]. The electrical resistivities of the samples were measured as a function of temperature from 300K to 1200K using a Linear Research LR400 4-wire bridge operating at 16Hz. Electrical contact to the films was made by wrapping nickel wire around the sample, and bonding the wires to the surface with silver paint. The thermocouple leads were held to the surface of the sample with the nickel wires, and bonded in place with the silver paint. Currents for the measurements were in the range of 1 to 100 mA.

### Thermal Conductivity

Room temperature thermal conductivity of Si/SiGe quantum well films were measured by the 3 $\omega$ -method. These measurements were done on two different groups of samples with similar results. The results are listed in Table 1. The bulk SiGe thermal conductivity measured in this modified 3 $\omega$  apparatus (Figure 1) yielded values within ~10% of published data.

In order to obtain the thermal  $\kappa$  in the plane direction (along the film) the film has to be instrumented on the edge as illustrated in the Figure 1. Values obtained by this technique (Table 1) indicate a large decrease (factor of 3) in  $\kappa_{in-plane}$  for the Si/SiGe quantum wells versus bulk material. These types of reduction in thermal conductivities are not unique and have also been observed by other investigators in other superlattices. For example Yao [8] and Yu [9] reported almost an order of magnitude reduction in  $\kappa_{in-plane}$  of GaAs/AlAs quantum wells compared to the bulk value. Also Chen [10] presented a thermal conductivity's model in superlattices which predicted a similar reduction in  $\kappa_{in-plane}$  of Si/Ge quantum wells.

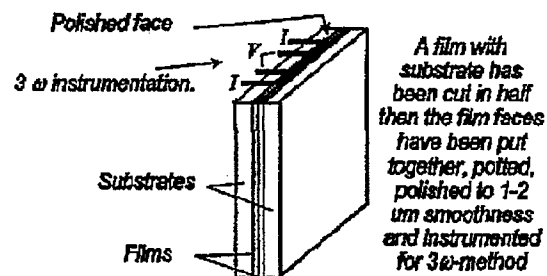


Figure 1. In Plane Thermal Conductivity 3- $\omega$  Method.

**Table 1. Thermal Conductivity of Si/Si Ge Film by 3 $\omega$ -method**

Sample	Published Bulk Thermal	Measured Film Thermal $\kappa_{in-plane}$ (W/cm <sup>2</sup> ·C)
P-type Si Ge	0.058	0.0129
N-type Si Ge	0.051	0.0135
Si	1.5	0.51

**N and P Couple**

A B<sub>4</sub>C/B<sub>5</sub>C-Si/SiGe P-N couple (shown in Figure 2) with low contact resistance was fabricated and the results appear very promising. Each leg in this couple consists of a square of 1000Å thick multilayer of B<sub>4</sub>C/B<sub>5</sub>C (P type) and Si/SiGe (N type) films. The films are deposited on 0.5 mm thick silicon substrate that is approximately 1cmx1cm. At a  $\Delta T=50^{\circ}\text{C}$  ( $T_{\text{cold}}=40^{\circ}\text{C}$  and  $T_{\text{hot}}=90^{\circ}\text{C}$ ), the voltage measured on this couple was ~ 0.1 Volts. The contact resistance was a few ohms which was very low compared to the total resistance of the couple which was approximately 20 k $\Omega$ . This is the resistance of the films and does not include the Si substrate [4, 5]. The results are tabulated in the Table 2. Efficiency was obtained as follows: (i) Power data,  $\alpha$  and  $\rho$ , were measured at a  $T_{\text{hot}} = 90^{\circ}\text{C}$  and  $T_{\text{cold}} = 40^{\circ}\text{C}$ . (ii) The Z for the couple, over the  $\Delta T = 90^{\circ}\text{C} - 40^{\circ}\text{C}$ , was calculated using bulk thermal  $\kappa$  property data. (iii) Efficiency was then calculated using the formulas 1 through 3.

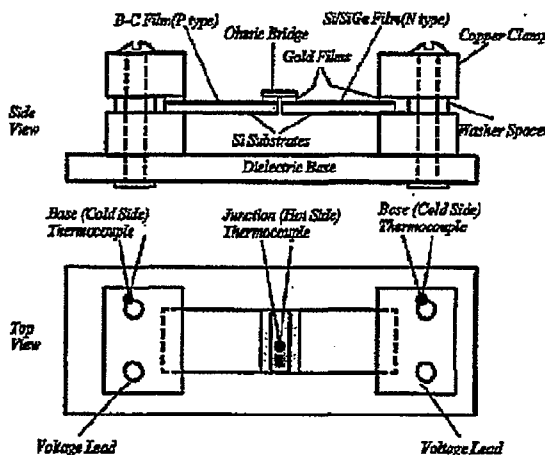


**Figure 2. Schematic of P-N couple test fixture.**

These values of voltage and resistance give a matched load power of about 0.125  $\mu\text{W}$  (micro-Watts) for the couple at a  $T_{\text{cold}}=40^{\circ}\text{C}$  and  $T_{\text{hot}}=90^{\circ}\text{C}$ . At these same temperatures and dimensions a bulk Bi<sub>2</sub>Te<sub>3</sub> couple produces only 0.01  $\mu\text{W}$ , a bulk B<sub>5</sub>C-SiGe couple produces only 0.004  $\mu\text{W}$ , and a bulk SiGe couple produces 0.02

$\mu\text{W}$ . Therefore the B<sub>4</sub>C/B<sub>5</sub>C-Si/SiGe P-N couple produces about ten times more power, than the bulk BiTe couple and about thirty times more power than bulk B<sub>5</sub>C-SiGe couple. Although this couple was fabricated with thin films (only 1000Å), Hi-Z hopes to duplicate these results with much thicker films (100,000Å) on a thinner or insulating substrate. Silicon substrates with thicknesses of 5 $\mu\text{m}$  (micro-meter) and 10 $\mu\text{m}$  are available commercially as are insulating substrates like Kapton. If fabrication of thick films on these substrates is successful then a 1cmx1cm couple, like the one described above, would produce 1250 $\mu\text{W}$  of power at a  $\Delta T=50^{\circ}\text{C}$ . The final goal is to fabricate and measure the properties of these thicker P-N couples on very thin or insulating substrates.

**THERMOELECTRIC FOR DIESEL ENGINES**

The auxiliary power requirements for heavy-duty trucks continues to increase. This will be particularly true when the power required to operate systems to reduce NO<sub>x</sub> and particulates are introduced. If something is not done to reduce the engine auxiliary power load, these cleanup systems could essentially double the auxiliary power requirements which will result in a significant increase fuel consumption.

Hi-Z has been working for several years to develop a system that can reuse the waste energy available in the engine's exhaust to provide the auxiliary power for the truck [11]. The system we are currently testing is shown in Figure 3 mounted on a class 8 truck in place of the muffler. This generator uses thermoelectric modules made of bismuth-telluride to convert the exhaust heat directly to 1kW of electricity with an efficiency of about 5%. A study of replacing the alternator with a 1kW thermoelectric generator completed in 1992 [12] showed that while the projected cost at the 1kW thermoelectric generator is more than a comparable alternator, the break even time for a class eight truck using such a system should be about two years in the United States and about eight months overseas.

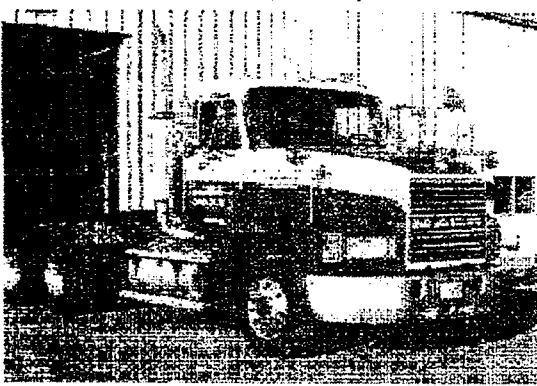


**Figure 3. 1kW Thermoelectric Generator Installed on a Class 8 Truck**

This study only considered replacing the alternator. However, there are gains in fuel economy to be made if some of the other engine driven auxiliaries can be replaced by electric driven components whose power is derived from waste heat rather than from the engine shaft.

These auxiliary devices could include the fan, power steering, power brakes, air compressor, NO<sub>x</sub> and particulate cleanup systems, and possibly air conditioning.

Figure 4 is an energy diagram for a typical present-day (96) Diesel engine. This figure also shows the same engine with a 5% efficient thermoelectric generator. One sees that the efficiency of the engine is increased almost two percentage points using the thermoelectric generator.

One has two choices to reduce the break even times. The first is to reduce the cost of the generator components and the second is to increase the system conversion efficiency.

Reducing component cost is difficult to do by itself. It can be more easily achieved, however, when the conversion efficiency is increased because one needs to transfer and convert less energy to provide the same output power. This results in fewer, smaller, and, therefore, cheaper

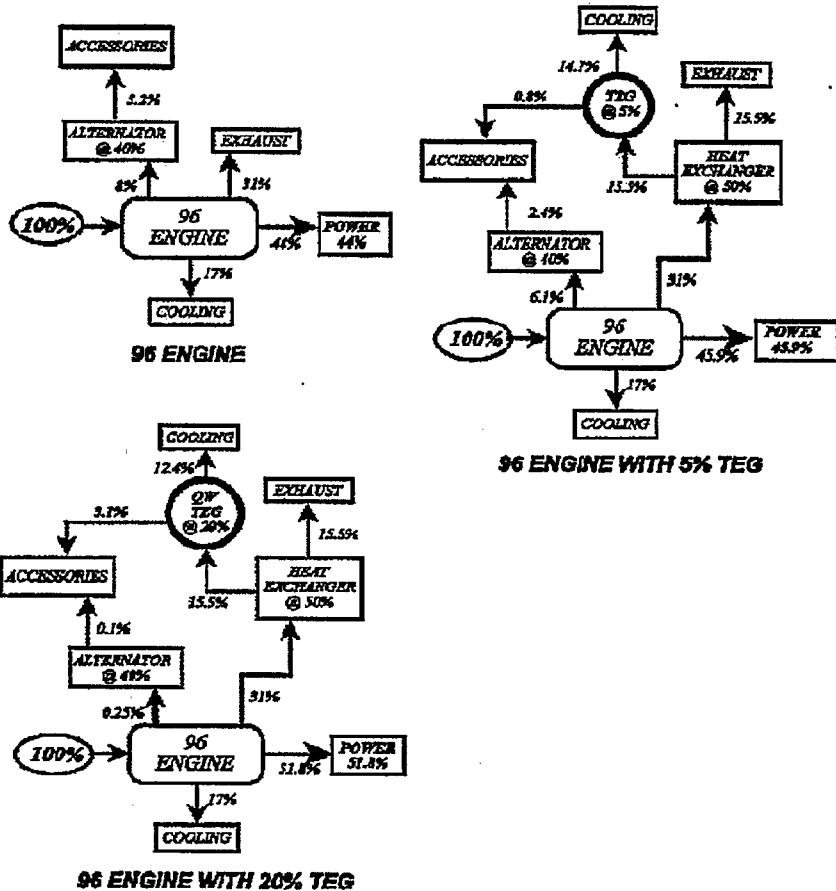


**Figure 4. Energy Diagram for 96 Engine with Thermoelectric Generator**

components are required which should result in a lower cost and, therefore, a shorter break-even time.

Hi-Z is approaching the problem of increasing system efficiency in two ways. The first is a near term program which should bear fruit within the next few months and the second is a long term program which may require several years to complete.

#### Near Term

The Jet Propulsion Laboratory in Pasadena recently announced [13] the development of zinc-antimonide ( $\beta\text{Zn}_2\text{Sb}_3$ ). The figure of merit ( $Z$ ) for several conventional P-type thermoelectric materials including zinc-antimonide are shown as a function of temperature in Figure 5. One can see that the  $Z$  for zinc-antimonide is higher than that for bismuth telluride above about 125°C. Since the energy conversion is proportional to the area under the  $ZT$  curve, the use of a P-type thermoelectric element made of a combination of bismuth-telluride on the cold end and zinc-antimonide on the hot end holds promise for a higher, greater conversion efficiency than using P-type bismuth-telluride alone in the 250 to 300°C range.

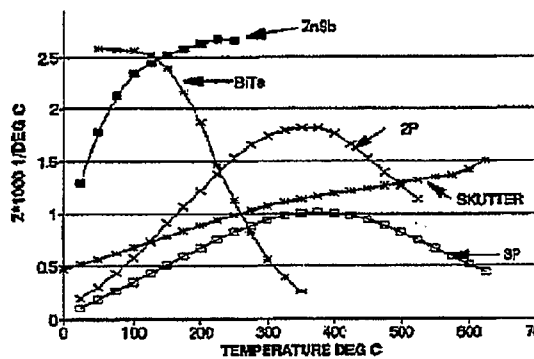


Figure 5. Figure of Merit Vs. Temperature for Several Thermoelectric Methods

Hi-Z and JPL are currently working on a program funded by DARPA to segment P-type zinc-antimonide and P-type bismuth-telluride to optimize the system conversion efficiency. If this program is successful, the module conversion efficiency will increase from 5% to about 7% which represents a 40% increase.

#### Long Term

Hi-Z has been developing multilayer quantum well (MLQW) thermoelectrics for several years. These materials consist of very thin (100Å) alternating layers of materials with two different electron band

gaps. When properly fabricated, the resulting material has very much improved thermoelectric properties compared to the same basic material made by conventional bulk methods.

Two types of MLQW systems have been discovered to date and both are now being developed under contracts to DOE. These systems are the silicon-germanium MLQW [14] and the boron carbon MLQW [15]. The silicon-germanium MLQW data indicate they will be used for cooling applications while boron carbon MLQW indicate they are good for power production. The boron carbon MLQW will be discussed first.

One of the problems that remain to be solved with the boron-carbon MLQW is that it can only be made as a P-type material. We are currently investigating other materials system to see if we can develop an N-type MLQW material with high temperature capability similar to that of the boron-carbon MLQW.

A conventional N-type bulk alloy such as bismuth-telluride can be used with the P-type boron-carbon MLQW materials to form the required couples. This will not result in conversion efficiencies as high as a system which uses both N- and P-type MLQW, however, the theoretical conversion efficiencies are still significantly higher than that provided by a system which uses only conventional bulk alloys. The current estimate is that a thermoelectric conversion system which uses a boron-carbon MLQW for the P legs and conventional bismuth-telluride for the N leg will have a conversion efficiency of about 20%.

The energy balance diagram shown in Figure 4 is for a present day (96) engine and a thermoelectric generator with a 20% energy conversion efficiency which can be achieved using the MLQW technology. In this case the overall energy efficiency is improved by a little over 7 percentage points or 17.7% compared to the standard engine.

Figure 6 shows the energy balance for a conventional LE 55 engine. Since there is less energy content in the exhaust of the LE 55 than the present day (96) engine, less energy is available for conversion. However, the inclusion of a thermoelectric generator with 20% efficiency would still improve the efficiency of the LE 55 by over 7 percentage points or 12.7%, as shown in Figure 6.

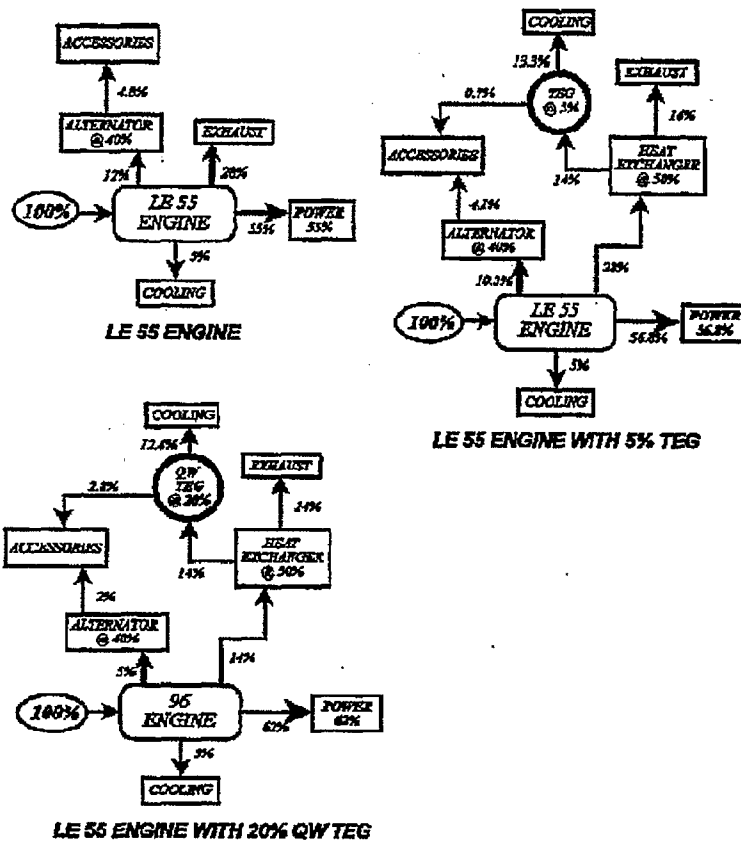


Figure 6. Energy Diagram of LE 55 Engine

It appears possible that the conversion efficiency of a MLQW device could be as high as 40% if a high temperature N-type materials can be identified. If that does happen, then the energy balance for the LE 55 with an advanced thermoelectric generator could be as shown in Figure 6. This energy balance shows a potential efficiency improvement of almost 10 percentage points or 18% over the LE 55's nominal 55 percent efficiency.

**Conclusion**

The overall engine efficiency of large Diesel engines can be improved by adding a thermoelectric generator to convert some of the energy available in the exhaust to useful electric energy. The overall percentage improvements which can be expected from current materials is low. However, new materials are being developed which can lead to significant improvements in overall engine efficiency over the next several years. Some of these materials will be available within a few months while more advanced materials will require several years of

development. Incorporation of these new thermoelectric materials should lead to a significant improvement in overall engine efficiency as well as a shorter break-even time. While the improvements expected are greater when thermoelectrics are applied to present day engines, it will also significantly improve the efficiency of the advanced LE 55 engine.

**Cost of Quantum Well Module**

Cost of a generator with 30% conversion efficiency modules will be about 10% of a generator with 5% conversion efficiency modules as it is shown in Figure 7. Conversely, for generators of the same size, the power output of a generator with 30% conversion efficiency modules will be about 10 times that of a generator with 5% conversion efficiency modules.

**ACKNOWLEDGMENTS**

This program was sponsored by the Department of Energy (DOE) under a Phase II SBIR grant with Dr. William Barnett the DOE Program Manager,

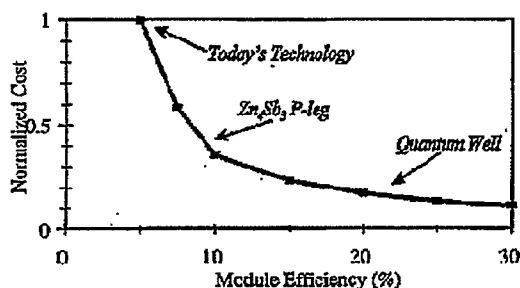


**Figure 7. Normalized module cost versus conversion efficiency for small generator.**

and Department of Defense (DOD) MURI program which Hi-Z is a subcontractor to UCLA with Dr. John Pazik the DOD Program Manager.

#### REFERENCES

1. Harman, T.C., "PbTeSe/BiSb Short Period Superlattices as a New Thermoelectric Cooling Material," *Proc. 1st Natl. Thermogenic Cooler Conf., Center for Night Vision and Electro-Optics*, U.S. Army, Ft. Belvoir, VA, 1992.
2. Hicks, L.D., Dresselhaus, M.S., "Thermoelectric Figure of Merit of a One Dimensional Conductor," *Phys. Rev. B* 47, 24 (1993) 16 631-634.
3. Hicks, L.D., Dresselhaus, M.S., "Effect of Quantum-Well Structures on the Thermoelectric figure of Merit," *Phys. Rev. B* 47, 19 (1993) 12 727-731.
4. N.B. Elsner, S. Ghamaty, J.H. Norman, J.C. Farmer, R.J. Foreman, L.J. Summersf, M.L. Olsen, P.E. Thompson and K. Wang, "Thermoelectric Performance of Si<sub>0.8</sub>Ge<sub>0.2</sub>/Si Heterostructures Synthesized by MBE and Sputtering" presented at XIII ICT, Kansas City.
5. S. Ghamaty, N. Elsner, K. Wang and Q. Xiang, "Thermoelectric Performance of B<sub>4</sub>C/B<sub>9</sub>C Heterostructures" presented at XIV ICT, March 1996, Pasadena, California.
6. N. B. Elsner, G.H. Reynolds, J.H. Norman and C.H. Shearer in "Boron-Rich Solids", AIP Conference Proceedings 140.
7. A. Ishizakkaland Y. Shiraki, *J. Electrochem. Soc.* 133(1986) 656.
8. Chen, G., M. Neagu, and T. Borca-Tasciuc, "Thermal Conductivity and Heat Transfer in Superlattices" in MRS Symposium Proceeding held March 31-April 3, 1997, San Francisco, California, U.S.A.
9. Yao, T., *Appl. Phys. Lett.*, 51, p. 1798-1800 (1987).
10. Yu, X.Y., G. Chen, A. Verma, and J.S. Smith, *Appl. Phys. Lett.*, 67, p. 3553-6356 (1995).
11. Bass, J.C., "Proof-of-Principle Test for Thermoelectric Generator for Diesel Engines", Final Report HZ72691-1, Hi-Z Technology, Inc., July, 1991.
12. Bass, J.C., R.J. Campana, and N.B. Elsner, "Evaluation of Novel Waste Heat Recovery concepts for Heavy Duty Diesel Engines", Final Report, HZ021191-1, Hi-Z Technology, Inc., February, 1991.
13. Caillot, T., J.P. Fleurial, and A. Borshchevsky, "Preparation and Thermoelectric Properties of Semiconducting Zn<sub>4</sub>Sb<sub>3</sub>", *Journal of the Physics and Chemistry of Solids*, V58, No. 7, Pp 1119-1125, Pergamon Press, 1977, Great Britain.
14. N.B. Elsner, et al "Thermoelectric Performance of Si<sub>0.8</sub>Ge<sub>0.2</sub>/Si Heterostructures Synthesized by MBE and Sputtering", *Proceedings of XIII International Conference on Thermoelectrics*, Kansas City, Mo August, 1994.
15. S. Ghamaty, N.B. Elsner, K. Wang, and Qi Xiang, "Thermoelectric Performance of B<sub>4</sub>C/B<sub>9</sub>C Heterostructures", *Proceedings XIV International Conference on Thermoelectrics*, Pasadena, California, March, 1996.

# Low $\Delta P$ Electrostatic Diesel Engine Nozzles

A. J. Kelly  
Charged Injection Corporation

## Introduction

To the extent that diesel engine performance and emissions behavior are controlled by atomization and mixing, the involvement of electrostatic effects will most assuredly provide a suite of options unavailable by any other means. Most importantly, these options have yet to be explored much less exploited. It is an interesting commentary on the state of diesel engine research to note that the first electrostatic nozzle has yet to be operated in even a single cylinder test engine. This is all the more striking in light of a robust scientific, technology and engineering base that exists for these nozzles; a base showing not only that there is no fundamental impediment to adaptation but that it represents "drop-in" technology to boot.

Mounting evidence, as exemplified by the recent work of Seibers (1), implicates mixing as the primary factor controlling diesel combustion. Contrary to conventional wisdom, atomization can no longer be considered to be the absolute determinant of fuel utilization. While all diesel atomizers provide adequate atomization, proper mixing certainly is the necessary and sufficient condition for vaporization and combustion, and may well be the dominant factor for emissions control. In light of this, consideration must be given to electrostatic atomization. Even if its other attributes are neglected, the hallmark of this process - vigorous droplet self-dispersion and attendant mixing - has to be considered in the quest for emissions control.

Quite bluntly, the purpose of this talk/paper is to challenge the engine community to at least consider the use of electrostatic atomization; its neglect to date is inexplicable and can no longer be justified on any rational basis.

## Electrostatic Atomization

A sense of the inherently unique options provided by electrostatic atomization for enhanced fuel/air mixing, and an appreciation of how electrical forces can contribute to the detailed control of combustion, can be garnered from consideration of the charged Jet-A plume depicted in Figure 1. For reference purposes, plume scale can be inferred by noting

that the single orifice atomizer, shown at the top of the image, is two centimeters in diameter.

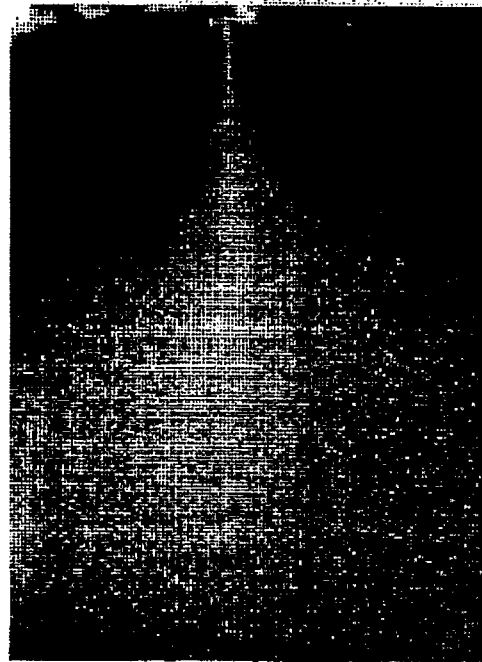


**Figure 1. Charged 0.9 mL/s Jet-A Plume, Issuing From a 250  $\mu\text{m}$  Diameter Orifice, 7 kV Input Voltage,  $\sim 2 \mu\text{A}$  Current.**

First, and most obviously, this and all charged droplet plumes differs from conventional, uncharged plumes insofar as a "spray cone angle" cannot be defined. In fact, the finest droplets generated close to the atomizer are not imaged, but actually are projected sideways at greater than  $180^\circ$ . A portion of these highly charged fines return to wet the grounded atomizer.

Second, droplet and plume development is purely electrostatic in nature. In the absence of electrical energization, the Jet-A issues as a straight, columnar stream from the 250  $\mu\text{m}$  diameter orifice.

Third, the atomization process is exceptionally efficient. Both atomization and dispersion are produced by approximately 14 mW of electrical input energy, corresponding to the 7 kV input

voltage and a spray current of  $\sim 2 \mu\text{A}$ . The hydraulic energy associated with the two atmosphere ( $\sim 200 \text{ kPa}$ , 30 psi) pressure drop simply serves to move the Jet-A through the device; it does not contribute to atomization nor does it aid dispersal. This is vividly illustrated by the ability of this device to operate at pressure differentials below 50 kPa (5 psi).

Fourth, the atomizer case is grounded; atomization and dispersal is solely due to the free electric charge in the exiting fluid. In fact, the electric field imposed by charge trapped in the fluid is limited by the background atmosphere breakdown strength. Fortunately, increased background pressure serves to elevate breakdown strength, permitting more charge to be imparted to the fluid. Consequently, increasing background pressure results in smaller droplet sizes, and enhanced dispersal. In addition, the droplet size distribution, which is inherently narrower than conventionally generated sprays, further narrows with pressure.

Fifth, droplet surface charge, by counteracting surface tension, functions as a surfactant and assists in droplet shattering.

Sixth, since charge injection occurs on microsecond time scales it is realistic to consider modulating the injection pulse to orchestrate the temporal and spatial placement of fuel within the combustion chamber. True electronic control can be exercised over the fuel air ratio through out the combustion chamber.

Seventh, and most remarkably, atomization and dispersion is independent of fluid properties and flow rate.

This last attribute requires some explanation.

Electrostatic spraying is the only atomization process quantitatively described by a first principles model (2). This model permits spray distributions (both droplet size and charge level) to be calculated with  $\sim 25\%$  accuracy without recourse to arbitrary constants. Briefly, mean droplet diameter ( $d$ ) for all Newtonian fluids and spray droplet sizes larger than  $\sim 1 \mu\text{m}$  can be shown to adhere to a simple rule:  $d(\mu\text{m}) = 75/\rho_e$ , where  $\rho_e$  is the charge density ( $\text{C}/\text{m}^3$ ,  $\mu\text{A}/\text{mL}/\text{s}$ ).

This law has been verified to within several percent accuracy for a wide variety of fluids, flow rates and operating conditions. As far as is currently known, mean droplet size (for purely electrostatic atomization) is completely independent of all factors save charge density, and reflects the quantum mechanical behavior of free charge on the droplet surface.

## Charge Injection Atomization

Questions concerning the basic physics of atomization notwithstanding, an immediate consequence of the theory is that high flow rate electrostatic atomization of all fluids could be achieved by directly charge injecting the spray fluid. All that need be done is to submerge an electron gun in the fluid to be atomized and dispersed; this is the SPRAY TRIODE<sup>®</sup> atomizer. Glossing over details covered in the references (2, 3), all charge injection atomizers exhibit the following behavioral characteristics:

- Droplet self-dispersivity
- Droplet size insensitivity to fluid properties, flow rate
- Narrow droplet size distributions
- Electronically controllable droplet size
- Enhanced droplet shattering

and provide unique opportunities for improved fuel preparation.

Extensive testing, in conjunction with theory (a first principles model of the SPRAY TRIODE atomizer (4) permits *ab initio* calculation of droplet size and charging distributions with  $\sim 25\%$  accuracy), provides assurance that existing diesel nozzles can be readily adapted to provide charge injection atomization and dispersion. This is illustrated by the cross sectional schematic of Figure 2.

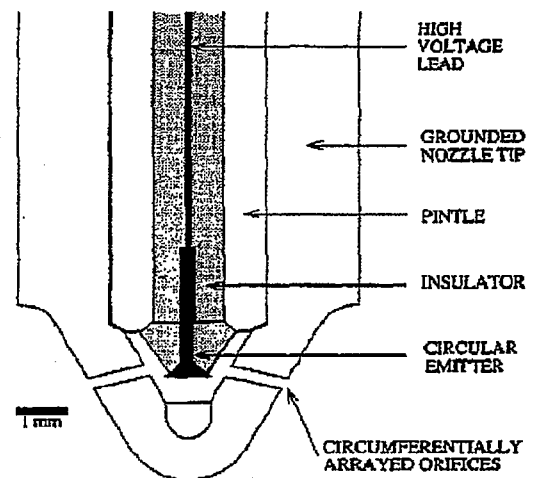


**Figure 2. Schematic of a Typical Multi-orifice Diesel Injector Converted to a Charge Injection Electrostatic Atomizer. All Orifices in the Circumferential Row are "Serviced" by a Single Emitter Electrode. Additional Rows of Orifices and Emitters can be Added to Further Reduce Delivery Pressure.**

For reasons explained in the literature, SPRAY TRIODE atomizer orifices typically fall in the 100 to 300  $\mu\text{m}$  diesel nozzle diameter size range. Consequently, since electrostatic atomization and dispersion are independent of flow rate, additional orifices and or slits can be added to satisfy the delivery requirement at a substantially lower pressure and pumping power level. Atomization/dispersion is decoupled from delivery requirements.

This capability is alluded to in the schematic of Figure 2 where a circular emitter electrode "services" a ring of eight or more orifices. Several such groupings can be readily accommodated within the confines of the sac region to form a very low pressure shower head nozzle. This is made possible by the fact that charge injection optimally occurs when the emitter/orifice entrance gap distance is approximately an orifice diameter. In other words, charge injection takes place within a volume having dimensions comparable to the orifice diameter. It is also worth noting that charged fluid can be transported without meaningful loss through orifices having substantially higher length to diameter ratios than those illustrated.

A special zirconia/tungsten emitter electrode assures reliable charge injection. These electrodes have proven to be exceptionally tough, resistant to degradation and straight forward to produce in arbitrary shapes. Other than this component, and the insulated high voltage wire required for energization, no other atomizer components have to be accommodated within the nozzle boundaries. Even if the rapid (MHz) response capability of these devices is used to tailor the spray/dispersion characteristics of the charged plume for optimal combustion/emissions reduction, total power requirements will be low. An instantaneous flow rate of 100 mL/s, charged to meaningfully high 4 C/m<sup>3</sup> level, by application of 10 kV corresponds to a per nozzle instantaneous power expenditure of 4 Watts. Average power will be correspondingly less. Cabin lights will draw more power than the electrostatic nozzles. But what can be expected of the charged nozzle?

#### Charged Plume Behavior

R. K. Avva of CFD Research Corporation has modified their proprietary CFD-ACE simulation code (5) to include a self-consistent description of charged droplet behavior for the purposes of evaluating the influence charging has upon diesel injection. Introduction of the long range electrical force, which places every charged droplet in communication with every other droplet in the

plume, makes simulations of this nature dauntingly complex and computationally intensive. Accordingly, the simulation was limited to dead top center of a 15:1 compression ratio truck engine with a chamber pressure of 4.4 MPa, 610°C temperature and a total nozzle flow rate of 0.1 L/s through 280  $\mu\text{m}$  diameter orifices. To lessen the computational burden, only one orifice was simulated and evaporation, but not combustion, taken into account. The droplet size distribution was taken to be that generated by a SPRAY TRIODE atomizer operating at 4 C/m<sup>3</sup>, that is droplets in the 20 to 60  $\mu\text{m}$  range with a distribution peak at approximately 52  $\mu\text{m}$ .

Figure 3 shows the progression, at 0.1 ms intervals, of a base-case, uncharged 268m/s injection velocity plume. Lateral droplet dispersion, starting approximately at 0.2 ms, is little amplified by the time the piston head/cylinder wall is encountered at the 0.4 ms mark. By contrast, modest droplet charging (4 C/m<sup>3</sup>) (Figure 4) immediately acts to expand the plume. Mixing is enhanced, particularly during the later phases of the injection pulse where a small contingent of droplets has flowed under action of the plume self-field to the cylinder head and is filling the far reaches of the chamber. Clearly charging is having a salutary effect on mixing and should positively impact combustion and emissions. This simulation supports the notion that by controlling charging level during the course of the injection pulse it will be possible to actively control combustion to meet specific ends.

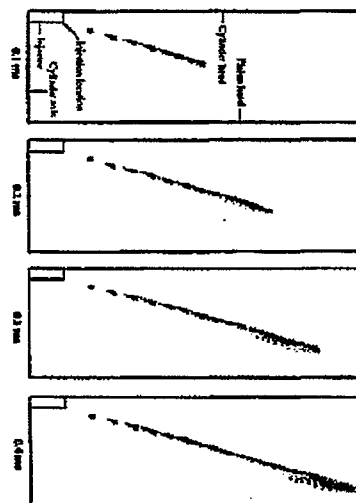
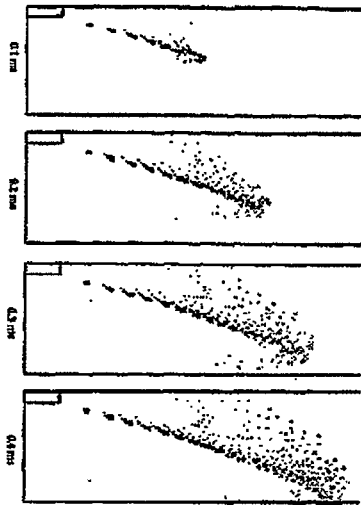
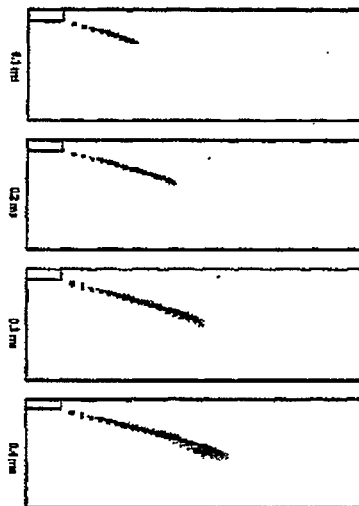


Figure 3. Uncharged Plume Development at 0.1 ms Intervals for Injection of 0.1 L/s Through a 280  $\mu\text{m}$  Orifice at 268 m/s in 4.4 MPa, 610°C Air



**Figure 4. Charged Plume ( $4 \text{ C/m}^3$ )**  
Development at 0.1 ms Intervals for Injection of 0.1 L/s Through a  $280 \mu\text{m}$  Orifice at 268 m/s in 4.4 MPa,  $610^\circ\text{C}$  Air, Compare to Plots of Figure 3.

In addition to providing new options to electrically control atomization/dispersion and combustion, charge injection atomizers offer another advantage. By decoupling, fluid delivery and atomization/mixing, a marked reduction in fuel delivery pressure and an associated reduction in equipment and pumping costs is possible. This capability will not only benefit existing engines, but has the potential to upgrade the large number of older, polluting diesels now in use world-wide.



**Figure 5. Uncharged Plume Development** at 0.1 ms Intervals for Injection of 0.1 L/s Through a  $280 \mu\text{m}$  Orifice at 100 m/s in 4.4 MPa,  $610^\circ\text{C}$  Air, Compare to Plots of Figure 3.

Computational limitations precluded simulation of plume behavior for injection velocities below 100 m/s. Nevertheless, such injectors would exhibit a seven-fold reduction in  $\Delta P$  relative to the existing, 268 m/s, example of Figures 3 and 4. Unsurprisingly, the uncharged 100 m/s plume (cf. Figure 5) exhibits markedly less lateral dispersion and penetrates 70% the distance of its 268 m/s counterpart. Again, the same plume droplet size distribution and chamber conditions are used. The situation is radically altered with the application of charging (Figure 6). Self-field repulsive effects, while only marginally improving penetration, act to explosively disperse the plume laterally to such an extent that it reaches both the cylinder and piston head. The peculiar "broccoli-like" appearance of the plume reflects a computational restraint requiring the use of an eight droplet size category histogram rather than a continuous profile.

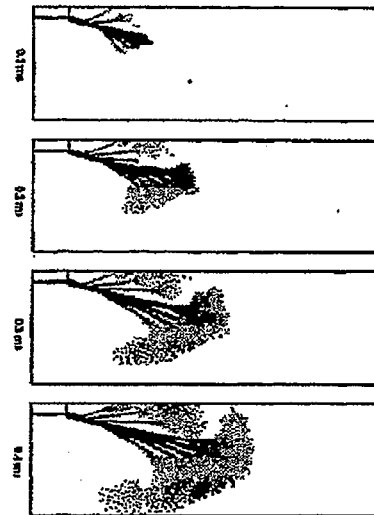


**Figure 6. Charged Plume ( $4 \text{ C/m}^3$ )**  
Development at 0.1 ms Intervals for Injection of 0.1 L/s Through a  $280 \mu\text{m}$  Orifice at 100 m/s in 4.4 MPa,  $610^\circ\text{C}$  Air, Compare to Plots of Figures 4 and 5.

As with all numerical simulations, criticism can be leveled that other assumptions or techniques would lead to different results. The essential point to be made is that while the details of the simulation can be legitimately questioned, there is little room to doubt that even small amounts of charging can produce globally significant enhancement in droplet dispersion/mixing.

## Summary

Electrical control of plume development and droplet mixing can be achieved by reconfiguring existing nozzles to directly charge injection fuel. The ability to obtain improved atomization/mixing/combustion at lower  $\Delta P$  will certainly lower engine cost, improve reliability and can have a salutary influence on emissions. The path is open for future engine designs in which electrostatic atomization obviates the need for turbulence and swirl (6).

## References

1. D. L. Seibers, "Liquid-Phase Fuel Penetration in Diesel Sprays", SAE paper 980809, Reprinted from Diesel Fuel Injection and Sprays (SP-1316), February, 1998.
2. A. J. Kelly, "Low Charge Density Electrostatic Atomization", IEEE Transactions on Industry Applications, IA-20, No. 2, pp. 267-273, March/April 1984.
3. A. J. Kelly, "On the Statistical, Quantum and Practical Mechanics of Electrostatic Atomization", J. Aerosol Science, 25, No. 6, pp. 1159-1177, 1994.
4. A. J. Kelly, "Charge Injection electrostatic Atomizer Modeling", Aerosol Science and Technology, 12, pp. 526-537, 1990.
5. R. K. Awa, CFDRC Private Communication, also M. Z. Pindera and M. G. Giridharan, "Numerical Studies of Acoustic Interactions with Spray Combustion", AIAA-94-0685, 32nd Aerospace Sciences Meeting & Exhibit, January, 1994.
6. J. Bellan and K. Harstad, "Dispersion (Electrostatic/Mechanical) and Fuel Property Effects on Soot Propensity in Clusters of Droplets", Atomization and Sprays, 7, 1998. Also, NASA Tech Briefs, p 64, April 1998.

# REAL-TIME MEASUREMENT OF DIESEL PARTICULATES

Kevin M. Morrison  
Electro-Mechanical Associates

## INTRODUCTION

Real-time measurement of diesel particulates is essential for optimizing fuel economy and driveability while controlling particulates on the various cycles prescribed by the Environmental Protection Agency. A rapid particulate assessment is needed because of the usual particulate overshoot when the load is ramped-up. The overshoot lasts only for a few seconds and thus makes steady measurements unrepresentative of transient operation.

This presentation describes a new, optically based particulate meter which is suitable for both light and heavy duty diesel engine applications, steady state or transient. It can also be useful for spark ignition engine development where particulates are a concern, i.e. direct injection combustion.

## BACKGROUND

Electro-Mechanical Associates (EMA) is staffed mainly by active or retired University of Michigan personnel from Mechanical Engineering and Applied Mechanics. For more than 5 years EMA has been partnering with a major heavy duty diesel manufacturer to construct a viable particulate meter capable of real time, on-line operation. That effort has resulted in the laser based meter described in this presentation. The meter has shown relatively good correlation with filter weights in both steady and transient tests. It has proven essential for use in NOx/particulate optimization strategies, for it is now possible to rapidly identify operating modes which produce high levels of particles. The meter has also been useful for identifying bad cylinders or injectors.

The particulate meter has been shown to be much more sensitive to low engine-out soot levels than existing opacity type smoke meters. This will be of increasing importance as regulations drive soot levels down further. Actually, the soot levels of today's engines are below the useful range of existing optical meters. Even filter weights are not very useful for engine development on the EPA transient cycle, due to the length of time required to get a measurable sample from a low emission engine and the particulate overshoot effect.

## TECHNICAL APPROACH

A laser beam reflects and scatters light from the particulates. This light is transduced by two photo-detectors. The signals from the detectors are processed to provide a measure of the particle concentration and the average size of the particles. The output is displayed in real time. Calibration is by comparison with filter weights. Steady mode and overall transient cycle results are obtained readily on a relative basis for a given engine, fuel and lubricant. Absolute values depend on the care of calibration, but relative values are usually sufficient for emission system development purposes. Because the EMA particulate meter is based on light reflection rather than attenuation, when compared to typical light extinction (opacity) meters, it is less prone to measurement error due to dirty windows or reduced light source output.

## CHARACTERISTICS

- Sample rate of 5 to 10 per second (100 - 200 ms).
- Responds well on the EPA Heavy Duty Diesel Emission Test Cycle
- Particle size down to 0.1 microns or less (important for health effects).
- Correlates primarily with dry particles (insolubles).
- The meter is relatively simple, low cost and does not require the degree of test cell sophistication required of filter weight measurement installations.
- Problems with sooting of the optical system and reflected "glare" are largely solved.
- Gives accurate directional information for a given engine, fuel and lubricant.
- Provides real-time particle size estimate.

## SUMMARY

With increasing emphasis on emissions and economy, many new engine and powertrain designs are evolving, such as direct injection

gasoline, light duty and utility diesel engines, and hybrids and vehicles with continuously variable transmissions. All these are potentially high particulate emitters either because of heterogeneous combustion or extended high load operation. Direct injection engines, either diesel or gasoline, exhibit increased particulates at high load and upon rapid increase of load. On transients the particulate increase lasts only a few seconds and depends, for example, on the volume of the intake manifold, turbo-charger delay, oxygen sensor and air meter response, and electronic control fuel strategy. Steady state filter weights do not give correct data for minimizing transient particulate emissions. It is very important to have real time data when tailoring such engines for minimum particulate emissions in real world driving and on the highly transient cycles prescribed by EPA.

#### REFERENCES

1. Anon., "Control of Air Pollution from Motor Vehicles and Motor Vehicle Engines", U.S. Code of Federal Regulations, v40, Part 86, July 1, 1986.
2. Anon., AVL Dynamic Particulate Analyzer DPA 480, AVL List GMBH.
3. Anon., Series 5100 Diesel Particulate Measurement System, Rupprecht and Patashnick Co. 1997.
4. Dobbins, R. A., Interactive Use of Electron Microscopy and Light Scattering as Diagnostics for Pyrogenic Aggregates", Proc. Materials Research Symp., v.250, 1990, pp. 101-106.
5. Graze, R. R. Jr., Development and Test of a Fractional Sampling System for Diesel Engine Particulate Measurement", ISA Chicago Tech. Conf., Sept. 20-23, 1993.
6. Jones, B. L., "In-Service Smoke and Particulate Measurements", SAE Paper 970748, SP-1248, 1997.
7. Kantola, T. C., et. al., "The Influence of a Low Sulfur Fuel and a Ceramic Particle Trap on the Physical, Chemical, and Biological Character of Heavy-Duty Diesel Emissions", ASE Paper 920565, 1992.
8. Kawai, T, et. al., "Real Time Analysis of Particulate Matter by Flame Ionization Detection", SAE Paper 980043, 1998.
9. Kerker, Milton, The Scattering of Light and Other Electromagnetic Radiation, Academic Press, New York, 1969.
10. Klingen H. J. and P. Roth, "Real Time Measurement of Soot Particles at the Exhaust Valve of a Diesel Engine", SAE Paper 912667, 1991.
11. Postula, A. and K. H. Lies, "Diesel Auto Particulates: A Chemical Characterization", Automotive Engineering, Feb. 1981, pp. 51-54.
12. Tree, D. R. and D. E. Foster, "Optical Measurements of Soot Particle Size, Number Density, and Temperature in a Direct Injection Diesel Engine as a Function of Speed and Load", SAE Paper 940270, 1994.